Design of Coplanar Waveguide Elliptic Low Pass Filters

Amjad A. Omar,[1] Nihad I. Dib,[2] Khelifa Hettak,[3] Maximilian C. Scardelletti,[4] Raed M. Shubair[5]

[1] Department of Communications Engineering, Hijjawi Faculty of Engineering Technology, Yarmouk University, Irbid, Jordan
[2] Department of Electrical Engineering, Jordan University of Science and Technology, Irbid, Jordan
[3] Communications Research Centre, Ottawa, Canada
[4] Microwave Metrology Facility, NASA Glenn Research Center, Cleveland, OH
[5] Department of Communication Engineering, Khalifa University of Science, Technology, and Research (KUSTAR), Sharjah, U.A.E

Received 16 October 2008; accepted 29 December 2008

ABSTRACT: This article proposes three design topologies of coplanar waveguide elliptic low pass filters. The design procedure is simple and explained in detail for the first topology. Numerical results are provided using the commercially available simulation softwares IE3D and HFSS to show the validity of the design with very good agreement. The proposed filters yield less than 0.1 dB attenuation in the passband (0–2 GHz), with a controllable slope of the transition between passband and stopband. The width of the rejection band is increased by simple filter cascading resulting in a passband to stopband ratio of up to 1:6. © 2009 Wiley Periodicals, Inc. Int J RF and Microwave CAE 19: 540–548, 2009.

Keywords: coplanar waveguide; low pass filters; elliptic filters

I. INTRODUCTION

Low pass filters (LPF) have been widely used to suppress undesired modes and spurious signals in nonlinear devices like mixers and frequency multipliers, etc. They have also been used to convert analog signals to band-limited signals before sampling and digitization [1].

Several types of low pass filters have been proposed in the literature. Among these are stepped impedance filters of the Chebyshev or maximally flat types [2]. These filters provide only a gradual transition from pass-band to stop-band and the discontinuities between the very high and very low impedance line sections degrade the filter performance. Recently, semi-lumped microstrip low-pass filters [3] were reported with a sharp cutoff frequency response. Unfortunately, soldering-lumped components will increase fabrication difficulties and also manufacturing repeatability is difficult to maintain. Low-pass microstrip filters using coupled lines [4] or stepped-impedance hairpin resonators [5] have finite attenuation poles in the cutoff frequency band. However, because the capacitance of the coupled lines is too small, the finite attenuation pole cannot be located close to the pass-band. Consequently, the cutoff frequency response is gradual. Dahlan and Eesa [6] reduced the size of the microstrip hairpin filter of [5] by using folded stepped impedance hairpin resonators. Arnedo et al [7] produced a microstrip filter with wide rejection band by periodically changing

Correspondence to: N. I. Dib; e-mail: nihad@just.edu.jo
DOI 10.1002/mmce.20376
Published online 26 June 2009 in Wiley InterScience (www.interscience.wiley.com).

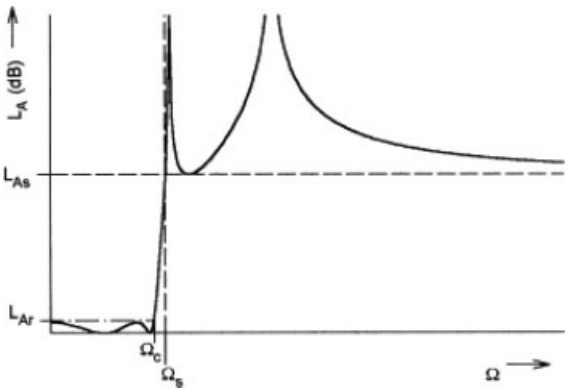

Figure 1. Ideal low pass filter response [17] (L_A is the attenuation in dB).

the width of a microstrip line in a sinusoidal fashion. Mandal et al. [8] used complementary split ring resonators to design compact, low insertion loss (IL), microstrip low pass filter with sharp cut-off. A new microstrip low pass filter using a defected ground structure (DGS) was also presented in [9–11].

In spite of the fact that coplanar waveguide (CPW) offers several advantages over microstrip due to its configuration, such as low radiation, low dispersion, ease of shunt and series connections, there is still a general lack of CPW filter designs and in particular CPW low pass filter designs. To this end, two maximally flat CPW LPFs were proposed by [12] using stubs with lumped resistive elements to improve matching. The use of lumped elements complicates the design and reduces its repeatability. Kaddour et al [13] proposed a new CPW LPF topology based on tapered periodic structures. In the area of elliptic CPW LPFs, a new elliptic EBG CPW LPF consisting of two sections of CPW transmission lines and one or more EBG cell was proposed in [14]. Using only one cell, this filter had about 1 dB insertion loss in the passband and stopband/passband ratio of 3/2 [14].

In this article, three different topologies of CPW elliptic LPFs are proposed. The design procedure is simple and the proposed LPF topologies possess very low passband ripple and controllable passband to stopband transition. In addition, the extent of the rejection band can be increased by simple filter cascading. The choice of elliptic filters as opposed to Chebyshev or maximally flat ones allows for a sharper transition between passband and stopband and smaller passband ripple.

Section II provides the filter specifications and the corresponding parameters of the lumped element elliptic low pass filter. Section III explains the first proposed CPW LPF topology and provides a detailed explanation of the design steps. It also provides the S-parameters of a one-section version of this filter obtained using two commercial simulators: IE3D [15] which uses the method of moments, and HFSS [16] which uses the finite element method. Section III also provides a three-section design of the same filter topology used to increase the attenuation and width of the rejection band. Sections IV and V explain the details of the second and third design topologies, respectively. Finally, conclusions are provided in Section VI.

II. ELLIPTIC LOW PASS FILTER (LPF)-LUMPED CIRCUIT

A. LPF Filter Specifications

Our aim is to design a CPW elliptic low pass filter with the following specifications: cutoff frequency f_c = 2 GHz, passband ripple L_{Ar} = 0.1 dB, stopband attenuation L_{As} = 18.8571 dB, and stopband starting frequency = 3.3898 GHz. Figure 1 shows the ideal response of an elliptic LPF where Ω is the normalized frequency f/f_c. Hence, in Figure 1, Ω_c = 1.0 and Ω_s = 1.6949.

The ideal elliptic function response shown in Figure 1 has the general transfer function:

$$|S_{21}(j\Omega)|^2 = \frac{1}{1 + \varepsilon^2 F_n^2(\Omega)} \tag{1}$$

where ε is the passband ripple and F_n (Ω) is given in eqs. (3)–(13b) of [17].

B. Low Pass Elliptic Filter-Lumped Element Circuit Parameters

The low pass elliptic filter-lumped element circuit is shown in Figure 2 [17]. Unlike the Butterworth and Chebyshev low pass prototype filters, there is no simple formula available for determining element values of the elliptic function low pass filter prototype [17]. Instead, some useful design data is available in Table (3.3) of [17] for equally terminated filter ($Z_o = Z_4$).

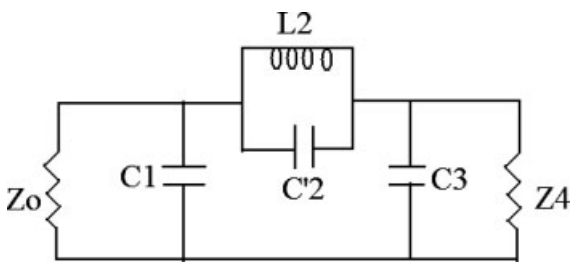

Figure 2. Elliptic low pass filter-lumped element circuit [17].

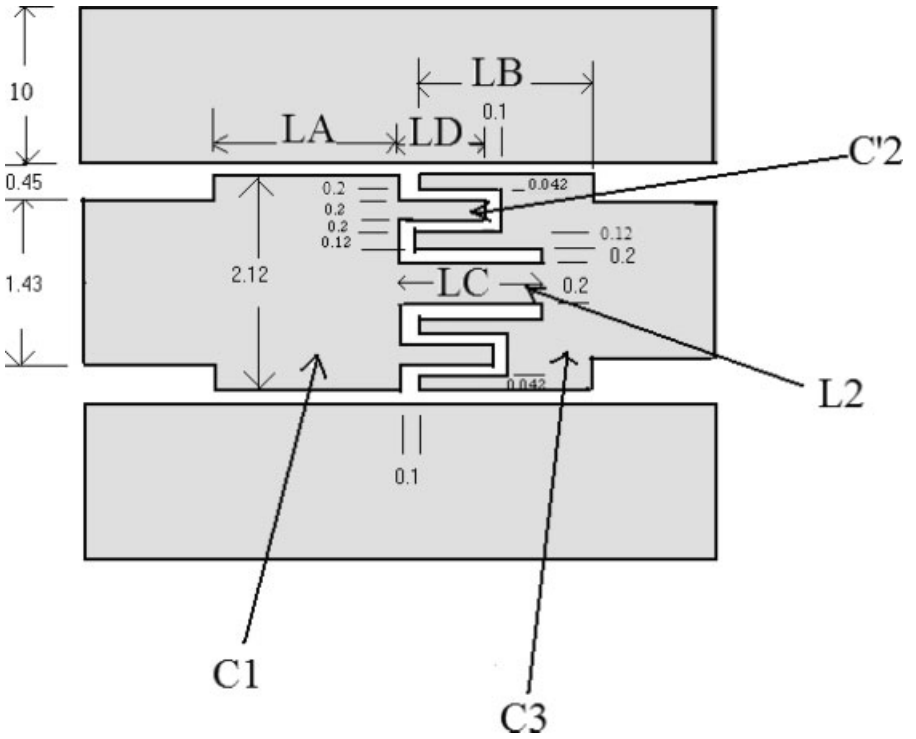

Figure 3. Design topology 1 (all dimensions are in mm).

Using this table, the lumped element values which yield the ideal response of Figure 1 for $L_{Ar} = 0.1$ dB, $\Omega_c = 1$, $\Omega_s = 1.6949$, and for unity feed and load impedances ($Z_o = Z_4 = 1\ \Omega$) are given by: $C_1 = C_3 = 0.8333$, $L_2 = 0.8439$, and $C_2' = 0.3252$.

The following frequency and load transformations [17] are applied to the prototype element values of Figure 2 to achieve the desired cutoff frequency ($f_c = 2$ GHz) and the desired feed and load impedance of $Z_o = Z_4 = 50\ \Omega$:

$$L_2 = \frac{Z_o L_2}{2\pi f_c} \tag{2}$$

$$C_i = \frac{C_i}{2\pi Z_o f_c} \qquad \text{for } C_1, C_3 \text{ and } C_2' \tag{3}$$

This results in $C_1 = C_3 = 1.33$ pF, $C_2' = 0.52$ pF, and $L_2 = 3.37$ nH. The goal is to implement these lumped elements using CPW circuits as explained below.

III. DESIGN TOPOLOGY 1

This topology is shown in Figure 3. The implementation of the elliptic LPF-lumped model of Figure 2 using CPW is achieved by replacing the two shunt capacitances C_1 and C_3 of Figure 2 with two CPW capacitive blocks consisting of a wide CPW transmission line having low impedance [2]. The series capacitance C_2' is replaced by a CPW interdigital capacitor, whereas the series inductance L_2 is replaced by a shorted CPW stub as shown in Figure 3.

A. Parametric Study of Topology 1

Before going through the design procedure, it is useful to perform a parametric study of this filter using

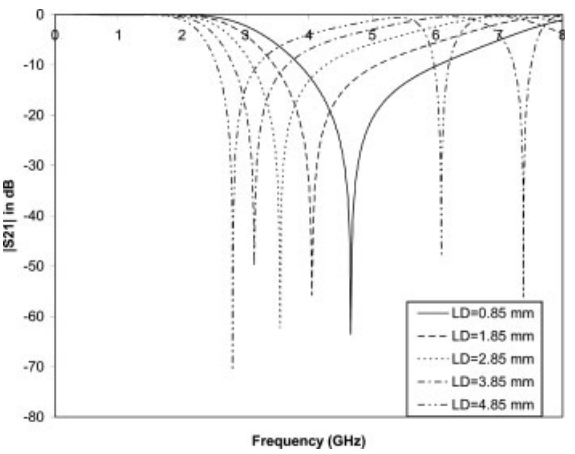

Figure 4. Effect of increasing the length L_D of Figure 3 ($L_A = 5.58$ mm, $L_B = 5.17$ mm, $L_C = 4.95$ mm).

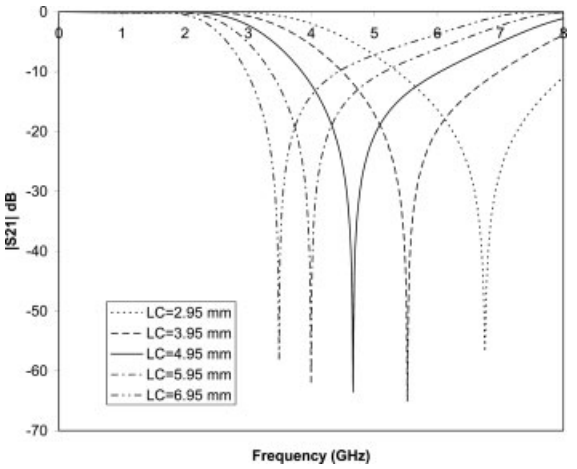

Figure 5. Effect of changing the length L_C of Figure 3 (L_A = 5.58 mm, L_B = 5.17 mm, L_D = 0.85 mm).

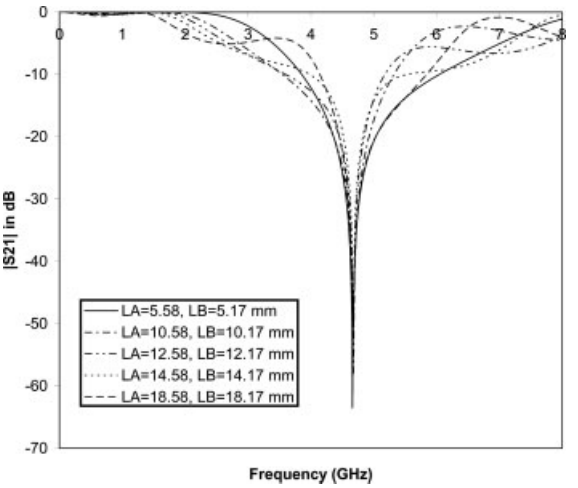

Figure 6. Effect of changing the lengths L_A and L_B of Figure 3 (L_C = 4.95 mm, L_D = 0.85 mm).

the commercial software IE3D [15]. For this particular topology, with no airbridges, IE3D solves for the magnetic current on the slots instead of the electric current on the entire conductor surface including the ground plane. This significantly reduces the computation time and memory [15]. Throughout the article, the dielectric substrate used is RT/Duroid 6010 having ε_r = 10.8 and thickness = 0.635 mm.

1. Effect of L_D. By increasing L_D, C_2' is increased (see Fig. 3). This causes a slight downward shift in the cutoff frequency (below 2 GHz) and a more significant decrease in the position of the first transmission null, and hence, an increase in the slope of the transition from passband to stopband. This is shown in Figure 4. Also, as L_D is further increased above 3.85 mm, a second transmission null appears inside the frequency range of interest [0–8] GHz. This effect will be useful when cascading several sections of this LPF as explained in Section (3.B).

2. Effect of L_C. The series inductance L_2 is predominantly controlled by the length LC of the shorted stub (see Fig. 3). Several simulations were also performed using IE3D [15]. Figure 5 shows that by increasing the length L_C, the cutoff frequency is reduced more significantly if compared with increasing L_D. Also, the first transmission zero is shifted downward and the slope of the transition from passband to stopband increases.

3. Effect of L_A and L_B. Figure 6 shows that increasing both C_1 and C_3 (by increasing L_A and L_B by same amount) causes a decrease in the cutoff frequency and an increase in the passband ripple. There is also a slight increase in the width of the stopband.

B. Design Procedure of a Single Stage LPF (Topology 1)

Initially, the substrate is chosen to be RT/Duroid 6010 having ε_r = 10.8 and thickness = 0.635 mm. Using the software Linegauge of Zeland [15], which has closed form quasi-static expressions for the effective dielectric constant and characteristic impedance of a general CPW, the slot width W and strip width S of the feed and load CPW lines are chosen to give a characteristic impedance of 50 Ω. This corresponds to S = 1.42 mm and W = 0.45 mm.

TABLE I. Design Steps of a Single Section LPF of Topology 1 [See Fig. (3)]

No.	$L_A = L_B$ (mm)	L_C (mm)	L_D (mm)	Im(Y11) (S)	Im(Y21) (S)	$C_1 = C_3$ (pF)	L_2 (nH)	C_2' (pF)
1	6.02	4.947	0.851	0.006286	0.02103	2.17	0.458	2.97
2	4.02	4.947	0.851	−0.00276	0.02016	1.38	0.47	3.05
3	4.02	4.947	1.151	−0.00225	0.01984	1.4	0.475	3.08
4	4.02	4.947	2.151	−0.00039	0.01869	1.46	0.493	3.2
5	3.52	4.947	3.151	0.00167	0.01745	1.52	0.513	3.33
6	3.52	4.947	3.151	−0.00042	0.01748	1.36	0.513	3.33
7	3.52	4.947	3.351	0.000024	0.01722	1.37	0.517	3.36

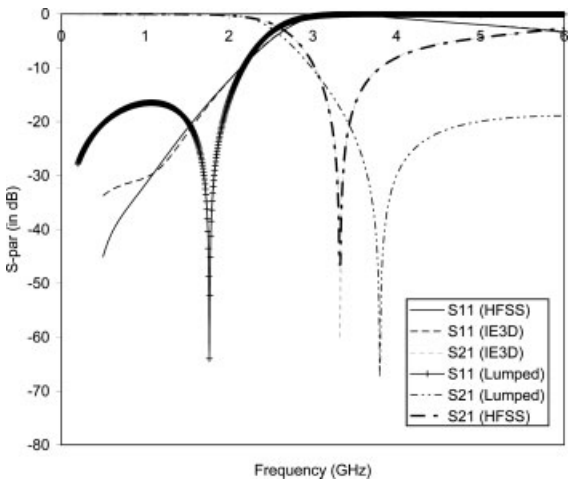

Figure 7. Simulated S-parameters of Topology 1, single stage, obtained using IE3D and HFSS ($L_A = L_B = 3.52$ mm, $L_C = 4.947$ mm, $L_D = 3.351$ mm).

An initial assumption of the lengths L_A, L_B, L_C, and L_D is made as shown in Table I, and the geometry of Figure 3 is simulated using IE3D [15] to obtain the 2-port Y-parameters of the CPW filter at the desired cutoff frequency of 2 GHz. From the Y-parameters, the elements of the lumped circuit of Figure 2 are calculated using the following simple formulas:

$$C_2' = \frac{A + \sqrt{A^2 + 4B}}{2} \tag{4}$$

$$L_2 = \frac{Z_o^2 g_2 C_2'}{g_2'} \tag{5}$$

$$C_1 = C_3 = \frac{\mathrm{Im}(Y_{11} + Y_{21})}{\omega_c} \tag{6}$$

where $A = -\frac{\mathrm{Im}(Y_{21})}{\mathrm{Im}(Y_{11})}$, $B = \frac{C_2'}{(\omega_c Z_o)^2 L_2}$, $g_2' = C_2$ and $g_2 = L_2$ as given in Section (2.B) before frequency and load transformations, and ω_c is the angular frequency at the cutoff frequency f_c.

The results of the first iteration are shown in Table I. The next step is to change the dimensions of L_A, L_B, L_C, and L_D in several iterations until our desired element values of Section (2.B) (i.e., $C_1 = C_3 = 1.33$ pF, $C_2' = 0.52$ pF, and $L_2' = 3.37$ nH) are obtained. This is shown in Table I.

The final design has the dimensions shown in iteration 7 of Table I. The S-parameters of this design are obtained using the two simulators IE3D and HFSS, as shown in Figure 7, with excellent agreement between the two simulators' results. This figure shows that the cutoff frequency is very close to 2 GHz, and the stopband starting frequency is also close to 3.3898 GHz. The drawback with this design is the small attenuation in the stopband (about 5 dB) and also the stopband to passband ratio is only about 2:1. The ideal-lumped element response is also shown in Figure 7. The agreement between the design and the lumped element response is excellent over the passband. However, in the stopband, the design exhibits less attenuation, smaller stopband starting frequency and smaller stopband to passband ratio.

This problem is solved by cascading three sections of the LPF filter as shown in Figure 8. The design of the three sections is simple where the left most sec-

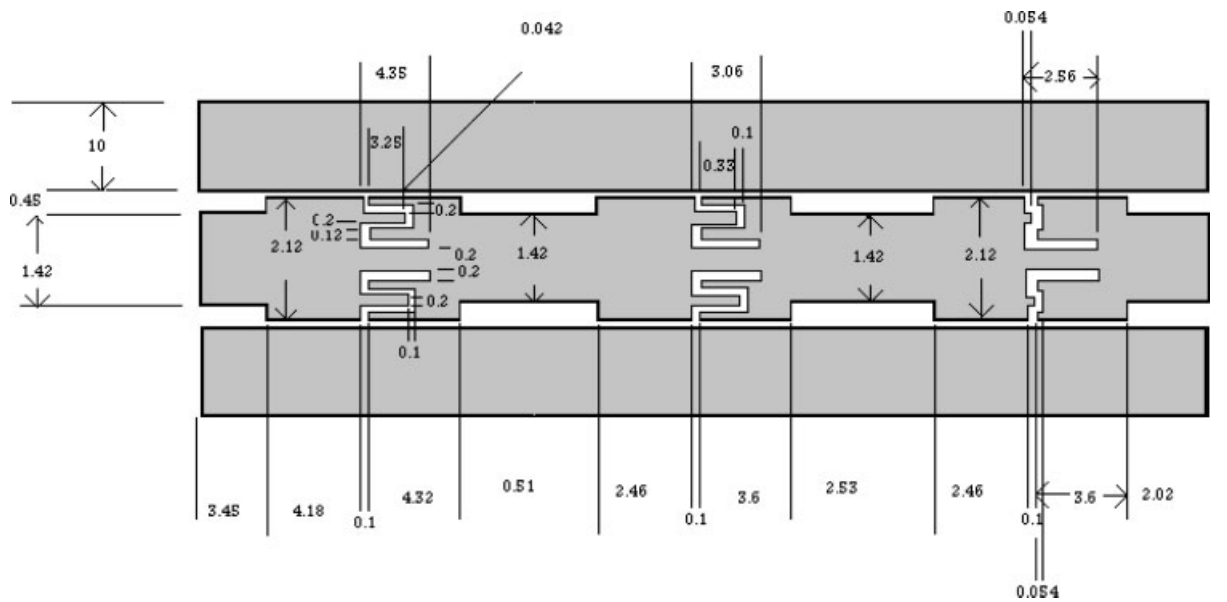

Figure 8. Topology 1, with three sections ($\varepsilon_r = 10.8$, $h = 0.635$ mm, all dimensions are in mm).

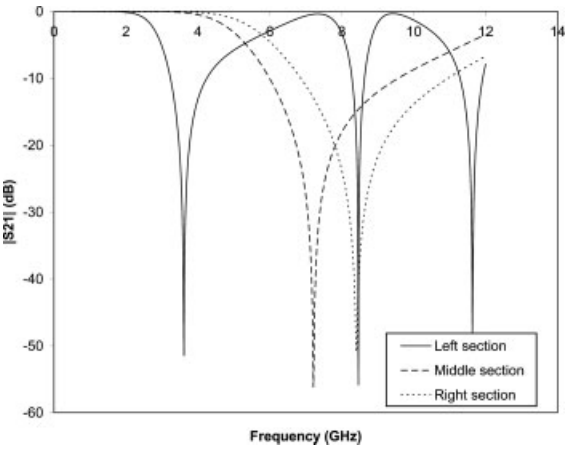

Figure 9. Response of each of the three sections of Figure 8 obtained using IE3D.

tion is designed first (alone) to have a cutoff frequency of 2 GHz and a sharp transition from passband to stopband ($\Omega_s \sim 3.3898$ as per design specifications). This follows the same procedure outlined in Table I. The middle and right sections are each designed individually such that the transmission peaks in the stopband of the leftmost section are cancelled by the transmission nulls of the stopband of the middle and right sections, as shown in Figure 9. The resulting S-parameters of the overall design are obtained using IE3D and HFSS and are shown in Figure 10. Here the stopband to passband ratio is increased to 6:1 and the attenuation in the stopband is below 20 dB. The overall size of the filter does not exceed 24 mm (0.83λ). The very close agreement between the results of the two simulators validates the accuracy of the results.

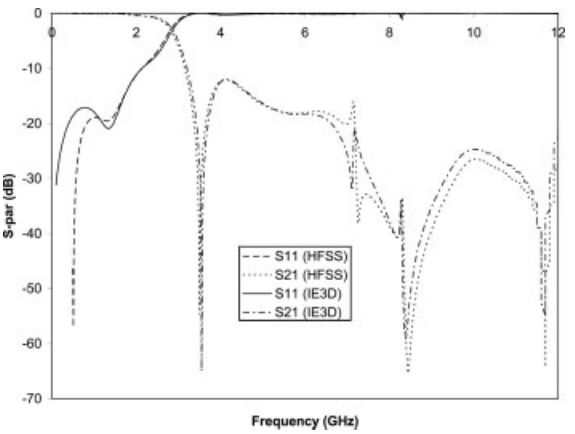

Figure 10. S-parameters of Topology 1 (three sections) of Figure 8.

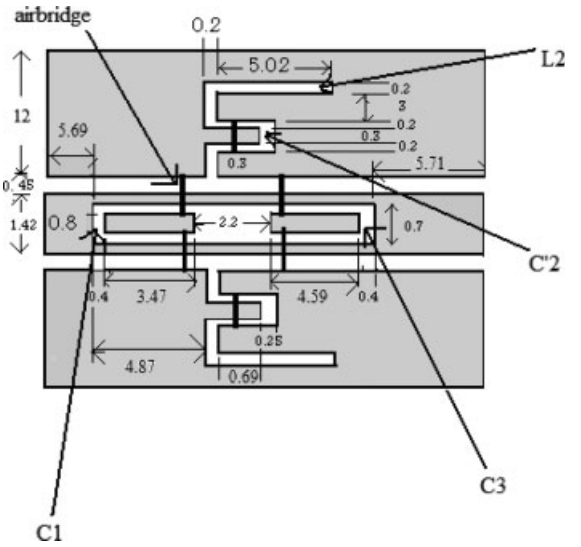

Figure 11. Design Topology 2, single section, with optimized dimensions ($\varepsilon_r = 10.8$, $h = 0.635$ mm, airbridge dimensions $h_a = 12$ μm, $W_a = 30$ μm, all dimensions are in mm).

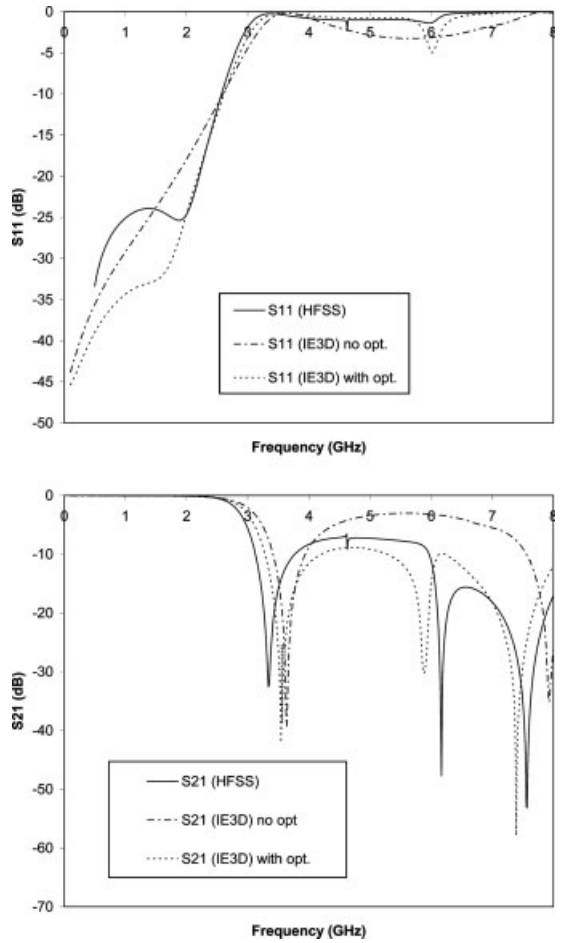

Figure 12. S-parameters of Topology 2 of Figure 11 with and without optimization (results of HFSS are with optimization).

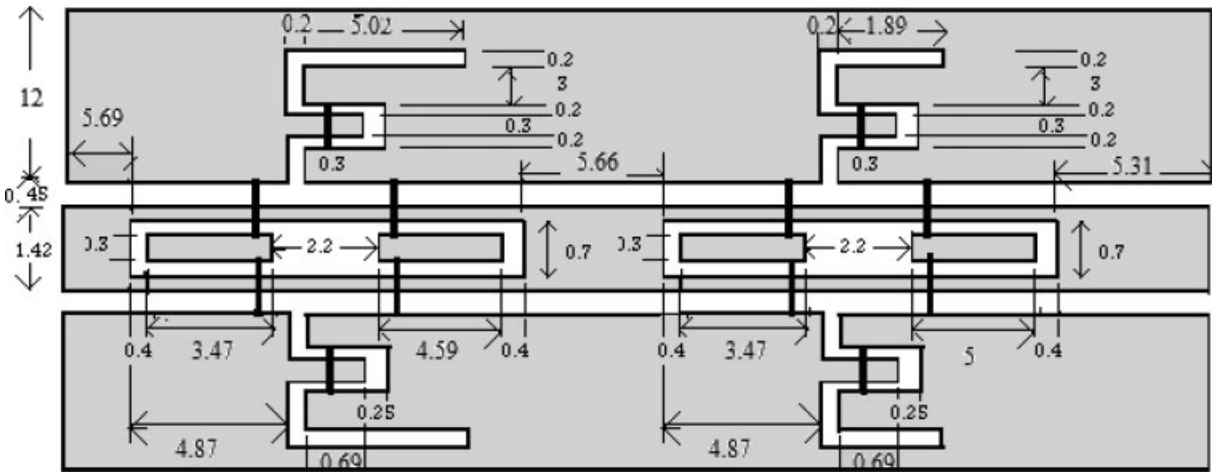

Figure 13. Topology 2 with two sections ($\varepsilon_r = 10.8$, $h = 0.635$ mm, airbridge dimensions $h_a = 12$ μm, $W_a = 30$ μm, all dimensions are in mm).

IV. DESIGN TOPOLOGY 2

This topology is shown in Figure 11. C_1 and C_3 are replaced by open ended stubs etched on the center conductor. L_2 is replaced by a short circuited stub etched in the ground plane, and C_2' is replaced by an open ended stub etched in the ground plane. Airbridges are used at different locations to tie the conductors to the ground plane at these locations and create shunt connections, as shown in Figure 11.

The design procedure is the same as that used for topology 1 except that after the initial design is achieved, optimization is used to improve the performance (i.e., reduce the attenuation in the stopband). Figure 12 shows the S-parameters obtained with and without optimization using IE3D and HFSS. Here the stopband to passband ratio is 4:1 and the passband attenuation is more than 10 dB.

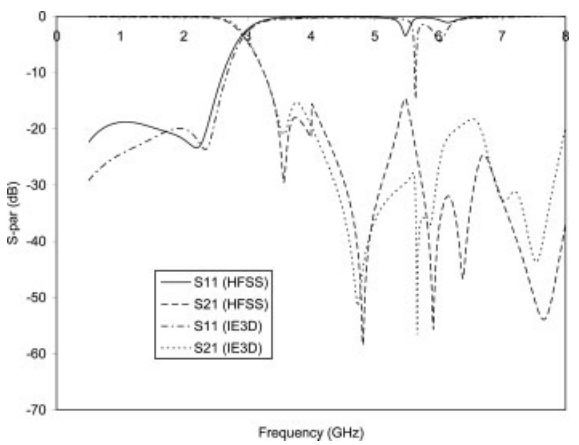

Figure 14. S-parameters of Topology 2 with two sections (Fig. 13) using IE3D and HFSS.

To increase the attenuation in the stopband, two sections of topology 2 are designed following the same procedure explained in Section (3.B). The two-section design is shown in Figure 13 with S-parameters obtained using IE3D and HFSS as shown in Figure 14. Here the attenuation in the stopband is more than 17 dB and the stopband to passband ratio is 4:1.

V. DESIGN TOPOLOGY 3

This topology with two sections is shown in Figure 15. C_1 and C_3 are replaced by two capacitive blocks generated by two wide CPW transmission line sections. L_2 is replaced by a current loop etched in the center conductor and generated with the aid of the

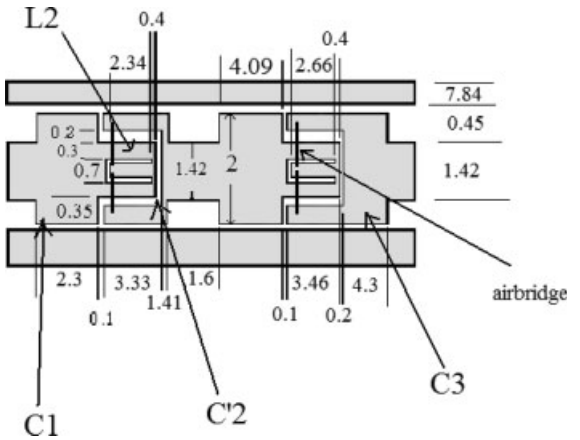

Figure 15. Topology 3 with two sections ($\varepsilon_r = 10.8$, $h = 0.635$ mm, airbridge dimensions $h_a = 10$ μm, $W_a = 30$ μm, U-slot is 0.2 mm wide, and all dimensions are in mm).

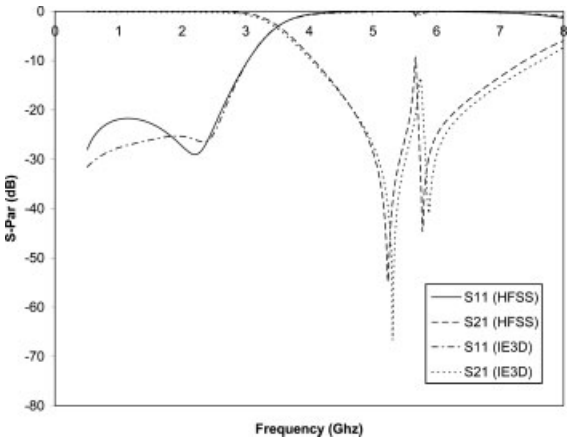

Figure 16. S-parameters of Topology 3 with two sections (Fig. 15).

airbridges, and C_2' is replaced by an open ended stub etched in the center conductor of the CPW.

The design procedure is the same as that used for topology 1 except that after the initial design is achieved, optimization is used to improve the performance (i.e., reduce the attenuation in the stopband). Figure 16 shows the S-parameters obtained after optimization using IE3D and HFSS. Here the stopband to passband ratio is 4:1 and the passband attenuation is more than 10 dB.

VI. CONCLUSIONS

This article proposed three different topologies of coplanar waveguide elliptic low pass filters. The designs are verified using the two commercial softwares IE3D and HFSS with very good agreement. A simple design procedure for each topology with one section is explained. More sections are used to increase the attenuation in the stopband and increase the width of the stopband.

It is clear from the different designs that, with one section only, the design specifications are not fully met. This is a result of the fact that distributed elements, especially at high frequencies, do not perform exactly the same as the corresponding lumped elements due to the different parasitic effects and dispersion.

REFERENCES

1. W. Tue and K. Chang, Compact microstrip low-pass filter with sharp rejection, IEEE Trans Microwave Theory Tech 15 (2005), 404–406.
2. D.M. Pozar, Microwave Engineering, Wiley, New-York, 1998, Chapter 8.
3. J.W. Sheen, A compact semi-lumped low-pass filter for harmonics and spurious suppression, IEEE Microwave Wireless Compon Lett 10 (2000), 92–93.
4. Y.W. Lee, S.M. Cho, G.Y. Kim, J.S. Park, D. Ahn, and J.B. Lim, A design of the harmonic rejection coupled line low-pass filter with attenuation poles, Asia Pacific Microwave Conf 3 (1999), 682–685.
5. L.H. Hsieh and K. Chang, Compact elliptic-function low-pass filters using microstrip stepped-impedance hairpin resonators, IEEE Trans Microwave Theory Tech 51 (2003), 193–199.
6. S.H. Dahlan and M. Esa, Miniaturized low pass filter using modified unifolded single hairpin-line resonator for microwave communication systems, Int RF Microwave Symp Dig (2006), 16–20.
7. I. Arnedo, I. Arregui, F.J. Falcone, M.A.G. Laso, and T. Lopetegi, Low pass filter with wide rejection band in microstrip technology, Int Symp Signals Syst Electron (2007), 13–16.
8. M.K. Mandal, P. Mondal, S. Sanyal, and A. Chakrabarty, Low insertion-loss, sharp-rejection and compact microstrip low-pass filters, IEEE Microwave Wireless Compon Lett 16 (2006), 600–602.
9. M.K. Mandal and S. Sanyal, A novel defected ground structure for planar circuits, IEEE Microwave Wireless Compon Lett 16 (2006), 93–95.
10. D. Ahn, J. Park, C. Kim, J. Kim, Y. Qian, and T. Itoh, A design of the low-pass filter using novel microstrip defected ground structure, IEEE Trans Microwave Theory Tech 49 (2001), 86–93.
11. N. Mollah, F. Hossain, J.S. Fu, and D. Yang, Novel technique of developing microstrip low pass filter (LPF), 6th International Conference on Information and Communications and Signal Processing, December 2007, pp. 1–4.
12. S. Khireddine, M. Drissi, and R. Soares, Flat group delay low pass filters using two CPW topologies, IEEE MTT-S Int Microwave Symp Dig (2005), 2215–2218.
13. D. Kaddour, E. Pistono, J. Duchamp, J. Arnould, and H. Eusèbe, A compact and selective low-pass filter with reduced spurious responses, based on CPW tapered periodic structures, IEEE Trans Microwave Theory Tech 54 (2006), 2367–2375.
14. K.S. Yee, Compact coplanar waveguide low pass filter using a novel electromagnetic band-gap structure, 7th International Conference on Antennas and Propagation & EM theory ISAPE, Guilin, China, 2006, pp. 1–4.
15. IE3D software of Zeland Inc. Available at: http://www.zeland.com.
16. HFSS software of Ansoft Inc. Available at: http://www.ansoft.com.
17. J. Hong and M.J. Lancaster, Microstrip filters for RF/microwave applications, Wiley, New York, 2001.

BIOGRAPHIES

Amjad A. Omar received the B.Sc. and M.Sc. in Electrical Engineering from Kuwait University in 1985 and 1988, respectively. He received the Ph.D. in Electrical Engineering from the University of Waterloo, Canada, in 1993. He worked at the Communications Research Center in Ottawa for 2 years (1993–1995). Since 1995, he has been working at several universities in the UAE and Jordan, and currently, he is an Associate Professor at the Communication Engineering Department of the Hijjawi College for Engineering Technology at Yarmouk University in Jordan. His research interests include computational electromagnetics, design of microwave and millimeter wave circuit components, biomedical applications of electromagnetics, and smart antennas. He has over 60 publications in various journals and refereed international conferences.

Nihad I. Dib obtained his B.Sc. and M.Sc. in EE from Kuwait University in 1985 and 1987, respectively. He obtained his Ph.D. in EE (major in Electromagnetics and Microwaves) in 1992 from University of Michigan, Ann Arbor. Then, he worked as an assistant research scientist in the radiation laboratory at the same school. In Sep. 1995, he joined the EE department at Jordan University of Science and Technology (JUST) as an assistant professor, and became a full professor in Aug. 2006. His research interests are in computational electromagnetics and modeling of planar microwave circuits.

Khelifa Hettak (M'05–SM'06) received the Dipl.-Ing. degree in telecommunications from the University of Algiers, Algiers, Algeria, in 1990, and the M.A.Sc. and Ph.D. degrees in signal processing and telecommunications from the University of Rennes 1, Rennes, France, in 1992 and 1996, respectively. In January 1997, he was with the Personal Communications Staff of the Institut National de la Recherche Scientifique (INRS)-Télécommunications. In October 1998, he joined the Electrical Engineering Department, Laval University, where he was an Associate Researcher involved in RF aspects of smart antennas. Since August 1999, he has been with Terrestrial Wireless Systems Branch, Communications Research Centre (CRC) Canada, Ottawa, ON, Canada, as a Research Scientist, where he is involved in the development of MMICs at 60 GHz, low-temperature co-fired ceramic (LTCC) packaging, and RF microelectromechanical systems (MEMS) switches.

Maximilian C. Scardelletti (S'96–M'99–SM'06) received the B.S.E.E. and M.S.E.E degrees from University of South Florida, Tampa, FL in 1997 and 1999, respectively. He is currently enrolled in Case Western Reserve University, Cleveland, OH where he is working towards a Ph.D. in electrical engineering. Maximilian is a senior research engineer with the Communications, Controls and Instrumentation Division at NASA Glenn Research Center in Cleveland, OH since 1999. He has authored and coauthored over 40 papers in refereed and symposium proceedings. His research interests include micromechanical (MEMS) devices, high temperature circuits and systems, and antenna design for wireless communications. Max is a senior member of IEEE and he is the chair for the IEEE Antennas and Propagation\Microwave Theory and Techniques Society Cleveland Chapter.

Raed M. Shubair received his B.Sc. degree from Kuwait University, Kuwait, in June 1989 and his Ph.D. degree from the University of Waterloo, Canada, in February 1993, both in Electrical Engineering. From March 1993 to August 1993 he was a Postdoctoral Fellow at the Department of Electrical and Computer Engineering, University of Waterloo, Canada. In August 1993 he joined Khalifa University of Science, Technology and Research (formerly Etisalat University College), UAE, where he is currently an Associate Professor at the Communication Engineering Department and Leader of the Communication and Information Systems Research Group. His current research interests include adaptive array and multichannel processing, smart antennas, and MIMO systems, as well as applied and computational electromagnetic modeling of RF and microwave circuits for wireless communications. He has published over 80 papers in refereed technical journals and international conferences. He has been a member of the technical program, organizing, and steering committees of numerous international conferences and workshops. Dr. Shubair is a founding member of the IEEE UAE Signal Processing and Communications Joint Societies Chapter. He currently acts as Symposium Vice-Chair of the 2008 IEEE Canadian Conference on Electrical and Computer Engineering: Communications and Networking Symposium. Dr. Shubair is Editor for the Journal of Communications, Academy Publisher. He is listed in *Who's Who in Electromagnetics* and in several editions of *Who's Who in Science and Engineering*.